A Robust Gradient for Long Wavelength FWI Updates

J. Ramos-Martinez* (PGS), S. Crawley (PGS), Z. Zou (PGS), A.A. Valenciano (PGS), L. Qiu (PGS) & N. Chemingui (PGS)

SUMMARY

We present a robust method to produce long wavelength updates in gradient-based Full Waveform Inversion (FWI). The solution introduces dynamic weights in the velocity sensitivity kernel derived from impedance and velocity parameterization of the classical objective function. The new kernel implementation effectively eliminates the migration isochrones produced by the specular reflections and enhances the low wavenumber components in the gradient in heterogeneous media. It is able to deliver velocity updates beyond penetration depth of diving waves. We use synthetic examples to illustrate how this dynamic weighted FWI gradient successfully recovers the velocity from pre-critical reflections. We also show with dual sensor data from deep-water Gulf of Mexico how the dynamic weighted FWI gradient can combine both transmitted and reflected energy in a global FWI scheme.

Introduction

Full waveform inversion (FWI) is the tool of choice for building high-resolution velocity models in shallow water settings. In this scenario, recorded refractions and diving waves allow FWI to resolve small-scale geologic features up to the deepest turning point. For deeper targets, FWI needs to rely on reflected energy to update the model. However, by using conventional gradient computations, FWI can only reconstruct the high-wavenumber components of the model unless the recorded data has ultra-low frequency content.

We propose a method to produce long wavelength velocity updates at greater depths by decomposing the gradient into separate wavenumber components (e.g., Xu et al., 2013; Zhou et al., 2015). The fundamental idea is to derive a gradient where the relatively high wavenumber migration isochrones corresponding to the specular reflections, are removed, and the low wavenumber energy is preserved. The new approach involves inserting dynamic weights in the velocity sensitivity kernel derived from an impedance-velocity parameterization. This eliminates the migration isochrones that dominate the gradient in heterogeneous media. Consequently, with the new gradient, we can update low wavenumber components in the velocity model beyond the penetration depth of diving waves. We first introduce the new FWI gradient and provide insight into its physical interpretation. Then, we show synthetic and field data examples where we use the new solution to build high resolution velocity models.

Theory

Conventional FWI (Tarantola, 1984) solves a nonlinear inverse problem by matching modeled seismic data to recorded field data. The matching is quantified by the residuals of a least-squares misfit function, and the model update is computed as a scaled representation of its gradient. In the case of an isotropic acoustic medium, parameterized in terms of bulk-modulus and density ($\boldsymbol{\kappa}$, $\boldsymbol{\rho}$), the gradient depends on the kernels for $\boldsymbol{\kappa}$ and $\boldsymbol{\rho}$ (Tarantola, 1984) that can be written, as:

$$K_{\kappa}(\mathbf{x}) = \frac{1}{\kappa(\mathbf{x})} \int \frac{\partial S(\mathbf{x},t)}{\partial t} \frac{\partial R(\mathbf{x},T-t)}{\partial t}\, dt, \quad (1) \quad \text{and} \quad K_{\rho}(\mathbf{x}) = \frac{1}{\rho(\mathbf{x})} \int \nabla S(\mathbf{x},t) \cdot \nabla R(\mathbf{x},T-t)\, dt, \quad (2)$$

where $\kappa(\mathbf{x}) = \rho(\mathbf{x}) v^2(\mathbf{x})$ is the equation that relates the bulk-modulus to velocity. In Equations 1 and 2, $S(\mathbf{x},t)$ and $R(\mathbf{x},t)$ are the source and residual wavefields. The sensitivity kernel for a particular parameter measures the variation in the misfit function caused by change in that parameter while holding the others fixed (Tromp et al., 2005). Figures 1a and 1b show the sensitivity kernels corresponding to Equations 1 and 2 in a model consisting of a single layer overlying a homogeneous half-space.

As an alternative, Douma et al. (2010) presented a velocity and impedance parameterization of the misfit function. The kernels corresponding to the new parameterization can be written as:

$$K_{v}(\mathbf{x}) = K_{\kappa}(\mathbf{x}) - K_{\rho}(\mathbf{x}), \quad (3) \quad \text{and} \quad K_{Z}(\mathbf{x}) = K_{\kappa}(\mathbf{x}) + K_{\rho}(\mathbf{x}). \quad (4)$$

The impedance kernel (Equation 4) comprises the high wavenumber components of the velocity field while the velocity kernel (Equation 3) is restricted to low wavenumbers (Luo et al., 2009). This realization gives an insight into the use of different kernels for different applications. The impedance kernel is useful for RTM where a high-resolution model is desirable and the velocity is fixed. On the other hand, the use of the velocity kernel is ideal for FWI where the low wavenumber components of the gradient are preferred while the high wavenumbers associated with reflections are problematic.

With the RTM application in mind, Whitmore and Crawley (2012) used the impedance sensitivity kernel (Equation 4) to derive an imaging condition capable of removing the unwanted backscattered noise. The examples presented in their paper, using heterogeneous models, highlight the importance

of dynamically weighting the different components of the impedance kernel to achieve optimal removal of the low wavenumber artifacts. Figure 1c shows the result of weighting the components from Figures 1a and 1b, to produce an RTM impulse response free of back-scattered noise.

Similarly, an FWI gradient can be derived by dynamically weighting the velocity sensitivity kernel (Equation 3). The dynamic weights of Whitmore and Crawley (2012) can be adapted to alternatively remove the high wavenumbers from the FWI gradient in a heterogeneous media. By assuming constant density the new FWI gradient can be derived from equation (3) as:

$$G(\mathbf{x}) = \frac{1}{2A(\mathbf{x})}\left\{\int_t \left[W_1(\mathbf{x},t)\frac{1}{v^2(\mathbf{x})}\frac{\partial S(\mathbf{x},t)}{\partial t}\frac{\partial R(\mathbf{x},T-t)}{\partial t} - W_2(\mathbf{x},t)\nabla S(\mathbf{x},t)\cdot\nabla R(\mathbf{x},T-t)\right]dt\right\} \quad (5)$$

where the dynamic weights $W_1(\mathbf{x},t)$ and $W_2(\mathbf{x},t)$ are designed to optimally suppress the migration isochrones, and $A(\mathbf{x})$ is the illumination term. Figure 1d is produced using equation 5; it illustrates how the migration smile has been removed while the low wavenumber energy is preserved.

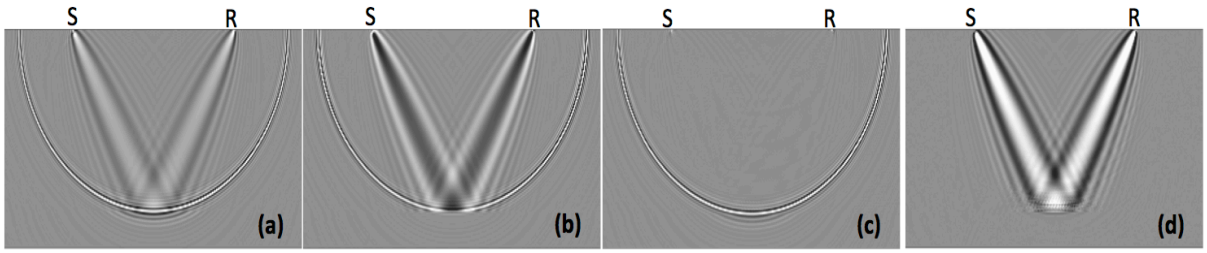

Figure 1 *Sensitivity kernels of a source-receiver pair in a model with a homogeneous layer overlying a half-space: (a) bulk-modulus, (b) density, (c) Impedance, and (d) velocity.*

Figure 2 shows the conventional FWI gradient (2a) compared to the modified gradient from Equation 5 (2b) for a model with a linearly increasing velocity with depth. Here, the modified gradient in Equation 5 removes the migration smile, but preserves all the low wavenumber components associated with the diving waves ("bananas") and backscattering "rabbit ears".

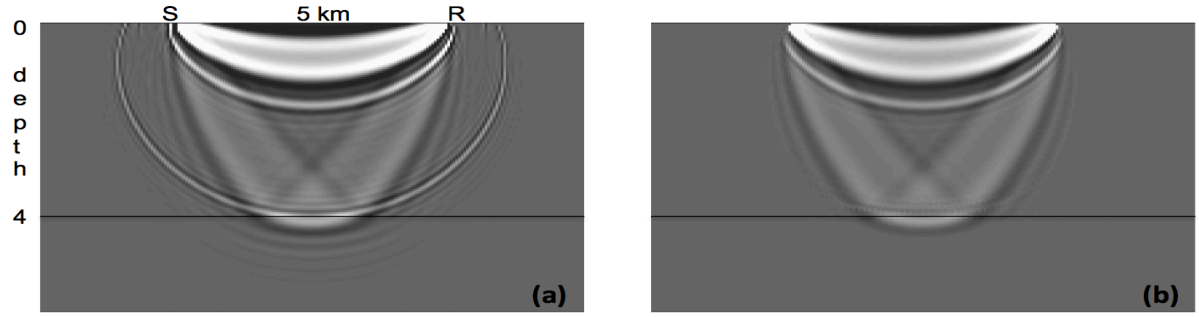

Figure 2 *Sensitivity kernels of a source-receiver pair in a model with a V(z) layer overlying a half-space: (a) conventional kernel and (b) dynamically weighted velocity kernel.*

Synthetic examples

We design a 2D synthetic example consisting of five homogeneous layers (Figure 3). The data has maximum offset of 4 km so only pre-critical reflections are used in the inversion. The starting velocity model for FWI contained errors up to 100m/s. The inversion was performed on a frequency band of 3-5 Hz. Figures 3b and 3c, show the results of the inversion using the conventional FWI gradient and the dynamic weighted FWI gradient. Results from the new FWI gradient are accurate and do not suffer from the high wavenumber artifacts observed on the conventional FWI update.

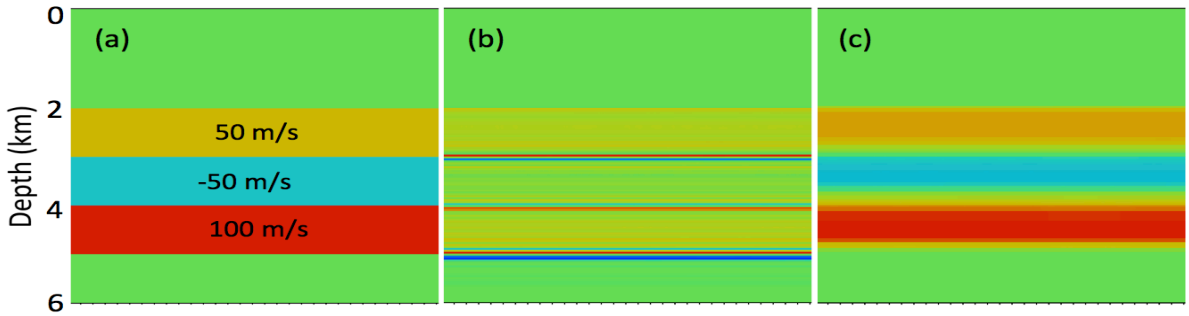

Figure 3 *Five layer synthetic model: (a) Difference between exact and starting model, (b) conventional FWI update, (c) new gradient velocity update.*

The second example uses a synthetic dataset inspired from a real earth model (Figure 4a). It consists of a smooth background velocity model that includes a meandering channel at 4 km depth. The maximum offset in the data is 4 km and the inversion was performed using a frequency band between 3-7 Hz. The background velocity model was used as starting model for FWI. Figure 4c shows the velocity model derived from the new gradient. Note that the 4km deep channel is nicely recovered using the deep reflections from the data with limited offsets up to 4km.

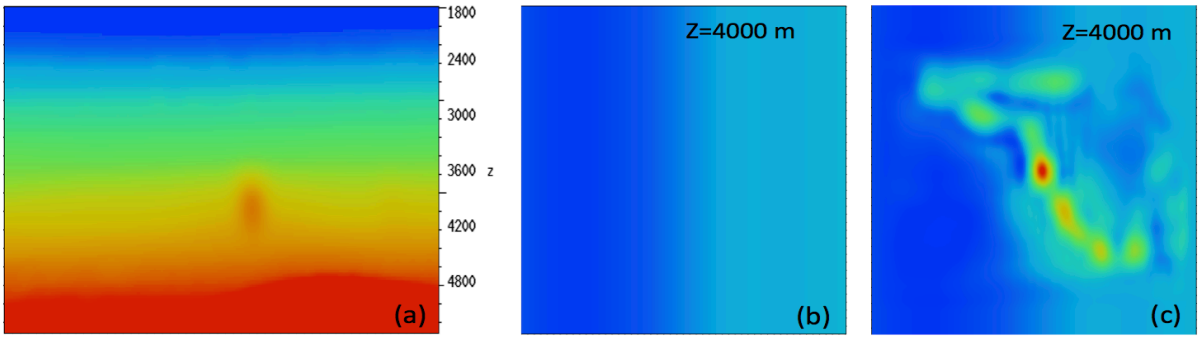

Figure 4 *3D synthetic example: (a) inline section from the true velocity model, (b) depth slice from starting model, (c) recovered FWI model using the new gradient.*

Field data example

We compare the dynamically weighted FWI gradient with the traditional FWI on field data from deep-water Gulf of Mexico (DeSoto Canyon). The data were acquired with dual-sensor streamers and with a maximum offset of 12 km. The FWI frequency band was 3-7 Hz. No particular mutes or event selection were used, therefore all recorded data were employed during the inversion. Figure 5a shows an overlay of the initial velocity model on the seismic image. Figures 5b and 5c show the updates from the conventional and the dynamically weighted gradients. Note how the new FWI gradient produces good resolution model updates that are free from high wavenumber artifacts. Also noticeable is the imprint of the seismic reflectivity on the conventional FWI updates. To further evaluate the model derived from the new gradient, we performed Kirchhoff depth migration. We observed that the new FWI velocity model improved the flatness of the offset gathers as shown in Figures 5d and 5e.

Conclusions

We present a novel solution for recovering the long-wavelength features in gradient-based FWI. The method uses reflected and transmitted wave modes to recover high-resolution velocity models. The new FWI gradient enables reliable velocity updates deeper than the maximum penetration depth of diving waves, and reduces the FWI dependency on recording ultra-long offsets.

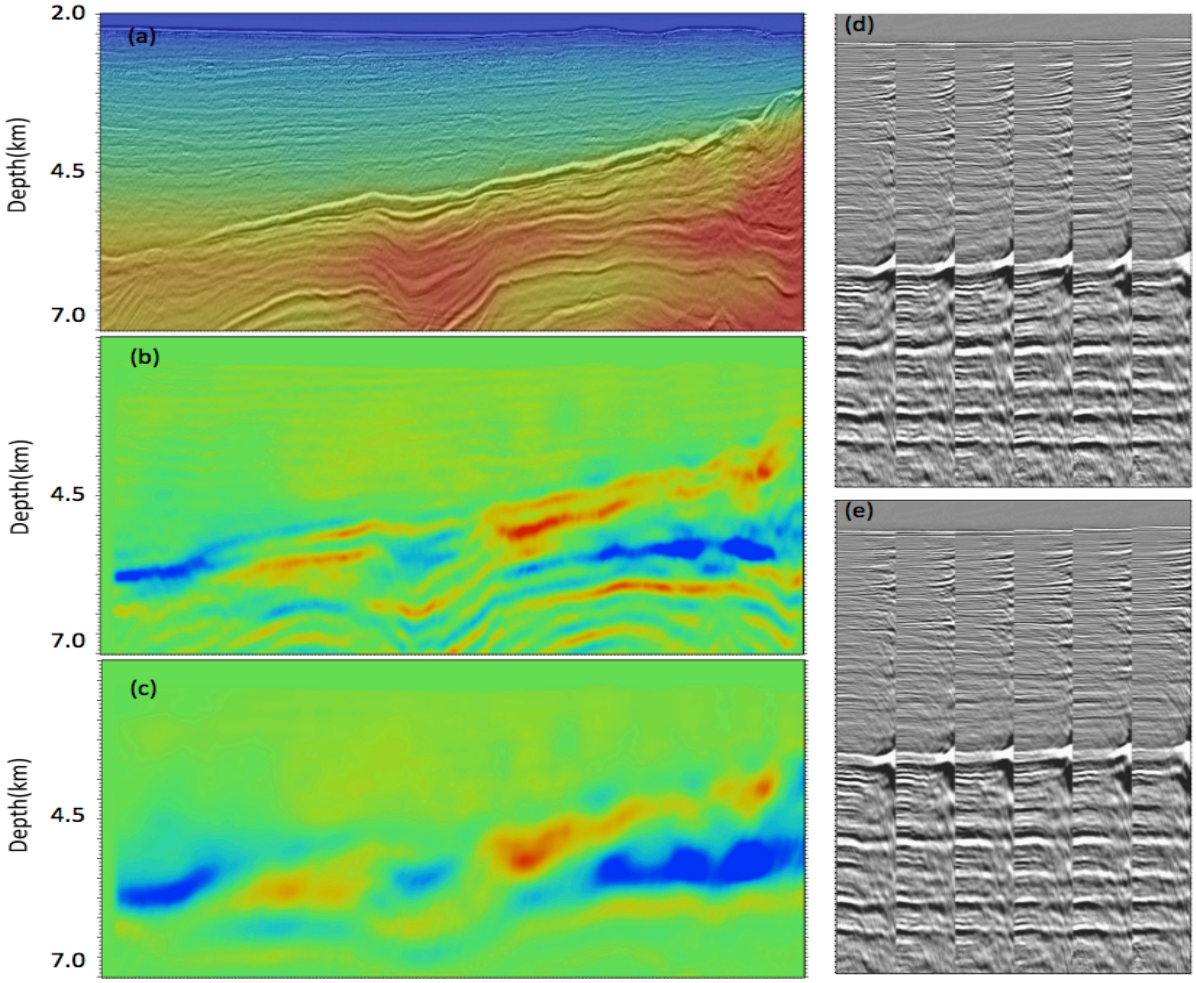

Figure 5 *Dual sensor data example from deep water Gulf of Mexico: (a) initial velocity model overlaid on the seismic image, (b) conventional FWI model update, and (c) new FWI model update. Kirchhoff offset gathers from: (d) initial velocity model, and (e) new FWI velocity model.*

Acknowledgements

We thank PGS for permission to publish the results. We thank Dan Whitmore for helpful discussions.

References

Douma, H., Yingst, D., Vasconcelos, I. and Tromp, J. [2010] On the connection between artifact filtering in reverse time migration and adjoint tomography, *Geophysics*, **75**, S219-S223.

Luo, Y., Zhu, H., Nissen-Meyer, T. Morency, C., Tromp, J. [2009] Seismic modeling and imaging based upon spectral-element and adjoint methods, *The Leading Edge*, **28**, 569-574.

Tarantola, A. [1984] Inversion of seismic reflection data in the acoustic approximation, *Geophysics*, **49,1259**-1266.

Tromp, J., Tape. C., Liu, Q. [2005]. Seismic tomography, adjoint methods, time reversal and banana-doughnut kernels, *Geophys. J. Int*., **160**, 195-216.

Whitmore, N.D. and Crawley, S. [2012] Application of RTM inverse scattering imaging conditions, 82nd Annual International Meeting*, SEG Expanded Abstracts*.

Xu, S., Wang, D., Chen, F., Zhang, Y., and Lambare, G. [2013] Full waveform inversion for reflected seismic data. *74th EAGE Conference & Exhibition, Extended Abstracts.*

Zhou, W., Brossier, R., Operto, S. and Vireux, J. [2015] Full waveform inversion of diving waves for velocity model building with impedance inversion based on scale separation, *Geophys. J. Int.*, **202**, 1535-1554.